Prediction of Blade Wake Interaction Noise Based on a Turbulent Vortex Model

Stewart A. L. Glegg*
Florida Atlantic University, Boca Raton, Florida 33431

Blade wake interaction is defined as the broadband noise generated by the interaction of helicopter rotor blades with their own wake. Experimental observations have shown that this is a strong function of advance ratio and tip-path plane angle. This paper describes how this noise source can be associated with the blade vortex interactions in the forward sector of the rotor. Measured levels of turbulence in the vortex core are used to predict the broadband noise levels with some success. However, more detailed information on the turbulence spectrum and the trajectory of the shed vortices is required before more accurate noise predictions can be made.

I. Introduction

A RECENT experimental investigation of helicopter rotor noise conducted in the Duits-Nederlandse aeroacoustic wind tunnel (DNW) has identified a new source of broadband rotor noise.[1] The tests were carried out on a 40% scale MBB B0-105 helicopter main rotor and considered a range of operational conditions, including variations in thrust, advance ratio, and tip-path plane angle. The results showed that the mid-frequency broadband noise was strongly affected by changes in tip-path plane angle (α_{ttp}) at constant thrust and advance ratio (Fig. 1). This led to the conclusion[1] that this source mechanism was the result of the interaction of the rotor blades with self-generated wake turbulence, which moves relative to the rotor disk with changes in tip-path plane angle and has been termed blade wake interaction noise (BWI). The time histories of BWI-dominated signatures[1] clearly indicated that this mechanism is quite distinct from impulsive blade vortex interaction noise (BVI) and persists at an almost constant level during each blade passage interval.

The results from the DNW test have been used to estimate the dominant contributors to the dB(A) and perceived noise levels (PNL) during a helicopter flyover.[2] These show that BWI is the most important noise source during level flight and mild climb conditions for this type of rotor. An understanding of this source mechanism is therefore crucial to the design of quiet helicopters. In particular, it may be that this mechanism is not significant in some rotor configurations, and hence, careful design of the rotor may eliminate this noise source.

In an earlier investigation, Munch et al.[3] identified broadband noise generated by local blade stall when the rotor passed close to trailing vortices. However, this only occurred at high rotor thrust levels and sudden increases of noise correlated with increases in drag. The tests in the DNW considered a range of rotor operating conditions including both low and high loadings, but changes in thrust caused relatively small-variations in noise levels. These observations were not consistent with the local blade stall effects described by Munch et al. and so this possibility is not included in the prediction method described here.

Brooks et al.[1] suggested that BWI is caused by the interaction of the rotor blades with the turbulence associated with the trailing vortices of the preceding blades. This paper considers this concept in more detail and develops a prediction method based on this idea. Good agreement is obtained with experimental measurements, within the limitations of the unknown aerodynamic parameters associated with the nonlinear motions of the trailing vortices.

The first part of this paper will consider the details of the blade wakes and how these interact with the rotor as a function of advance ratio, thrust, and tip-path plane angle. This shows that the blade vortex interactions that are responsible for impulsive (BVI) noise are concentrated in the rear sector of the rotor disk, and their axial displacement from the path of the blades is very sensitive to changes in α_{ttp}. The blades also intersect vortices in the forward sector of the rotor, but this does not cause BVI impulses since the intersections are normal to the direction of blade motion, and so do not cause sudden changes in lift. These intersections are less sensitive to changes in α_{ttp}, and it is postulated that the turbulence associated with these interactions is responsible for broadband BWI noise. This concurs with the directional microphone observations,[4] which show BWI noise to be located in the forward sector of the rotor on the advancing side.

A noise prediction scheme based on this concept is derived in Sec. III. For this, it is necessary to have a detailed knowledge of the turbulence associated with the vortex, in particular, the spatial variation of the turbulence intensity and the integral length scale. Information on this is found in wind-tunnel tests on nonrotating airfoils, described in Sec. IV, and gives the best available estimates of the correct order of magnitude of these variables, since at this time the effect of blade rotation on vortex core turbulence has not been measured. In Sec. V, the noise prediction scheme given in Sec. III is combined with the wake predictions described in Sec. II and the estimated turbu-

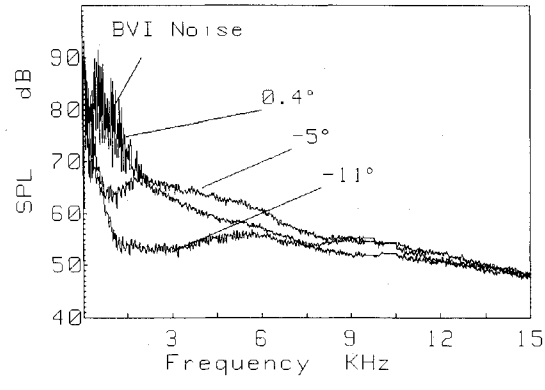

Fig. 1 Measured spectra from the rotor noise test in the DNW for advance ratio $\mu = 0.173$. Frequency resolution = 17.5 Hz.

Presented as Paper 89-1134 at the AIAA Aeroacoustics Conference, San Antonio, TX, April 10-12, 1989; received May 8, 1989; revision received May 16, 1990; accepted for publication Aug. 1, 1990.

*Associate Professor, Department of Ocean Engineering. Member AIAA.

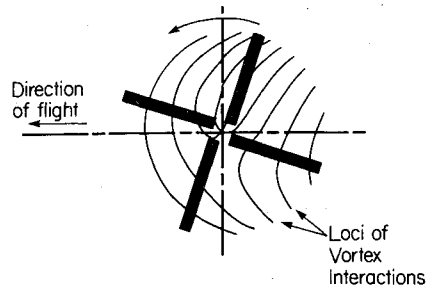

Fig. 2 Potential blade vortex intersections for a four-bladed rotor with an advance ratio of $\mu = 0.173$.

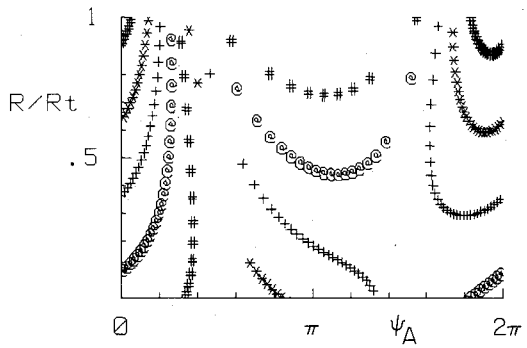

Fig. 3 Radial locations of blade vortex intersections in rectilinear format as a function of azimuthal location ψ_A for a four-bladed rotor ($\mu = 0.173$).

lence parameters. The results are then compared with the experimental measurements, and conclusions drawn about the accuracy of the method and its sensitivity to the estimated parameters.

II. Rotor Wake

When a helicopter is in forward flight, the rotor operates in the proximity of its own wake, and this would appear to be the most significant cause of inflow velocity fluctuations. The wake behind each blade is composed of two parts, namely, the velocity deficit behind each blade and the tip vortex. It is well known that the tip vortex is responsible for strong BVI impulses in certain flight regimes, but the cause of broadband blade wake noise is not well defined, and the purpose of this section is to consider the different aspects of the rotor wake that may be responsible for this noise source.

First, we will consider the tip vortex wake close to the rotor disk since this part of the flow is expected to be associated with the largest velocity fluctuations encountered by the blades. When a helicopter is in forward flight, the tip vortices are ingested into the rotor and blade vortex interactions occur. These interactions will depend on the local aerodynamics and the vortices will be displaced from their mean flow location by the passage of the blades. To first order, the potential blade vortex intersections can be estimated from the mean flow and the unsteady induced downwash.[5] A typical chart illustrating blade vortex intersections is shown in Fig. 2, for a four-bladed rotor with an advance ratio of $\mu = 0.173$. Strong blade vortex interactions occur in the rear sector of the rotor on the advancing side, where the vortex intersection lines are normal to the direction of blade motion. It is also important to note that weak blade vortex interactions occur in the forward sector of the rotor, and that in this sector the vortex from the preceding blade is approximately parallel to the blade motion. This interaction will not cause an impulsive acoustic signature, but may be responsible for a persistent source of unsteady flow, which can generate broadband noise.

One of the important features of BVI and BWI noise is its dependence on the rotor tip-path plane angle. This strongly affects the axial displacement of the vortices from the rotor

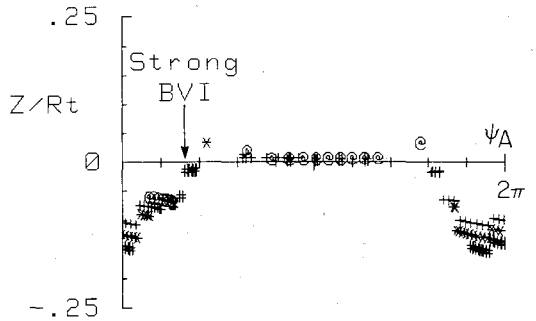

Fig. 4 Axial location of blade vortex intersections at $\alpha'_{tip} = 0.4$ deg as a function of azimuthal location ψ_A. The corresponding radial locations are shown in Fig. 3.

plane, and hence the strength of the blade vortex interactions. The axial displacement of the vortices may be calculated, using the mean axial flow and a distorted wake correction. The axial displacement z is given by

$$z/R_t = \lambda_T \psi_w + \Delta z/R_t \tag{1}$$

where R_t is the blade radius, λ_T is the rotor inflow ratio, ψ_w is the wake age of a particular vortex specified in radians and represents the time since the vortex was shed. The correction factor $\Delta z/R_t$ allows for the induced flow from the shed vorticity and is defined by

$$\Delta z/R_t = E(\psi_w, \mu, C_T) G(\psi_A) \tag{2}$$

where $E(\psi_W, \mu, C_T)$ is the generalized wake envelope function, $G(\psi_A)$ is the generalized wake shape function,[5] and ψ_A specifies an angular location in the rotor disk plane.

The rotor inflow ratio can be obtained from

$$\lambda_T = \mu \sin\alpha'_{tip} - (C_T/2)\left[(\mu \cos\alpha'_{tip})^2 + \lambda_T^2\right]^{-1/2} \tag{3}$$

and is the only parameter in Eq. (1) that depends on the corrected tip-path plane angle α'_{tip}. (Note that the actual tip path plane angle α_{tip} must be corrected for mean flow distortion effects that occur during wind tunnel testing.)

The axial displacements of the vortex intersections as a function of blade azimuthal location ψ_A are shown in Figs. 4 and 5, for a four-bladed rotor with an advance ratio of $\mu = 0.173$ and a thrust coefficient of $C_T = 0.0044$, at two different tip-path plane angles. By using the method next described, the strength of these BVIs can be evaluated from Fig. 3, which gives the radial location of the vortex intersections as a function of azimuth angle for the same conditions in a rectilinear format. The blade may be considered a vertical line moving linearly from left to right in Fig. 3 parallel to the ψ_A axis. Note how the intersections in the range $0 < \psi_A < \pi/2$ give vertical lines in Fig. 3 and so are almost parallel to the leading edge of the blade and hence cause strong BVIs, whereas those in the range $\pi/2 < \psi_A < 3\pi/2$ are nearly normal to the leading edge of the blade and so cause weak BVIs. The axial displacements of these intersections (Figs. 4 and 5) show how the strengths of the BVIs will change with rotor tip-path plane angle. Figure 4 shows that when $\alpha'_{tip} = 0.4$ deg, the strong BVIs at $\psi_A = \pi/4$ lie close to the tip-path plane ($z/R_t = 0$), and so a strong interaction that generates an impulsive acoustic signature is expected. However, as α'_{tip} is reduced to -11 deg, the axial displacement of these BVIs becomes significant, and since the amplitude of the acoustic BVI signatures decays rapidly with the vortex displacement from the blade path, strong acoustic signatures will not be generated in these regimes. The intersections in the forward sector of the rotor $\pi/2 < \psi_A < 3\pi/2$ are less sensitive to changes in tip-path plane angle. When $\alpha'_{tip} = 0.4$ deg (Fig. 4), these intersections are clustered close to the tip-path plane ($z/R_t = 0$), but when $\alpha_{tip} = -11$ deg (Fig. 5), the intersections occur at larger axial displacements. The minimum axial dis-

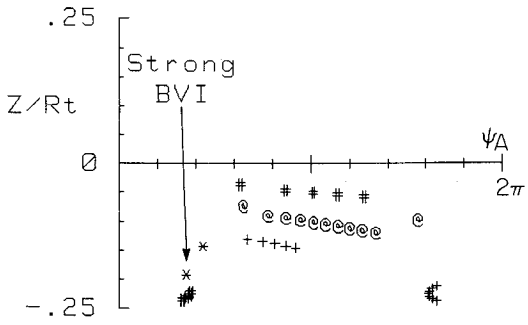

Fig. 5 Axial location of blade vortex intersections at $\alpha'_{tip} = -11.1$ deg as a function of azimuthal location ψ_A. The corresponding radial locations are shown in Fig. 3.

placements at $\psi_A = \pi$ are 0 and $0.8c$ (where c is a typical blade chord length) for $\alpha'_{tip} = 0.4$ deg and -11 deg, respectively, and so the blades will clearly be affected by the flow in the vortex core in each case.

The acoustic measurements shown in Fig. 1 are consistent with these observations. First, the BVI noise is a maximum for the smallest value of α'_{tip} and is eliminated at larger angles. Second, the BWI noise is much less sensitive to changes in α'_{tip}, with the highest levels occurring when $\alpha'_{tip} = 0.4$ and -5 deg and lower levels at $\alpha'_{tip} = -11$ deg. It would therefore appear reasonable to develop a noise prediction scheme based on the premise that BWI is generated by weak blade vortex interactions in the forward sector of the rotor where the vortex axis is nearly normal to the leading edge of the blade. However, to do so, it is first necessary to consider in detail the turbulent velocity fluctuations associated with trailing tip vortices, and how these generate broadband rotor noise.

III. Acoustic Analysis

To estimate the spectra of BWI noise, a prediction scheme has been developed based on the methods given by Amiet,[6] Paterson and Amiet,[7] Glegg,[8] and Glegg et al.[9] The noise is assumed to be produced by the interaction of the blade with the turbulence in the core of the trailing vortices of the preceding blades. The scale of this turbulence is taken to be much smaller than the rotor diameter so the resulting acoustic spectrum will be broadband[10] in nature and periodic components in the flow, which can cause noise at rotor harmonics, are assumed to be slowly varying so that they have an insignificant effect at the frequencies of interest. The purpose of this prediction scheme is to calculate the power spectral density of the acoustic pressure measured in the farfield of the rotor. To this end, we will use the method given by Paterson and Amiet[7] and Glegg,[9] which computes the broadband noise spectrum from the instantaneous power spectrum generated by the blade as it moves over the rotor disk plane. These references,[6-9] however, consider the blade to be immersed in a region of turbulence that is larger than the blade span, whereas here we are concerned with a blade that is only partially immersed in turbulence. This leads to some important simplifications in the analysis that predicts the noise field, and consequently the complete analysis will be given here.

Consider a blade of chord c and infinite span that is moving uniformly with velocity U. The blade encounters turbulence that has a velocity distribution $w_i(\xi)$, and the observer is taken to be at η in a stationary frame of reference. The blade surface may be specified in the moving coordinate system $\gamma = \xi - U\tau$, where τ is source time, so that the unsteady velocity encountered by the blade as a function of time is $w_i(\gamma + U\tau)$. The distance between the surface and the observer at source time τ is given by $r = |\eta - \xi| \approx r_0 - \eta \cdot (\gamma + U\tau)/r_0$, where $r_0 = |\eta|$.

The acoustic field that results from the interaction of the blade with inflow turbulence may be specified in terms of unsteady lift and unsteady thickness noise.[9] The unsteady lift component is described by the Ffowcs Williams and Hawkings equation for a blade that lies in the $\xi_3 = 0$ plane as

$$p_3(\eta,t) = \frac{\partial}{\partial \eta_3} \int_0^c \int_{-\infty}^{\infty} \left[\frac{\Delta p(\tau,\gamma)}{4\pi r |1 - M_r|} \right] d\gamma_1 \, d\gamma_2 \tag{4}$$

where the terms in square brackets are evaluated at source time $\tau = t - r/c_0$, $\Delta p(\tau,\gamma)$ is the unsteady surface pressure jump applied to the blade on the airfoil planform surface, and M_r is the Mach number of the blade in the direction of the observer.

The unsteady surface pressure jump may be specified in terms of the two-dimensional wave number spectrum of the inflow gust velocity, defined as

$$\hat{w}_i(k_1,k_2) = \frac{1}{(2\pi)^2} \int_{-R_1}^{R_1} \int_{-R_2}^{R_2} w_i(\xi_1,\xi_2,0) e^{-ik_1\xi_1 - ik_2\xi_2} \, d\xi_1 \, d\xi_2 \tag{5}$$

where R_1 and R_2 define the turbulent region. To obtain the unsteady surface pressure, this must be convolved with the airfoil gust response function $g(\gamma_1,k_2,k_2)$ as specified by Amiet.[6] For an airfoil moving with velocity $U \equiv (-U,0,0)$ so that $\xi_1 = \gamma_1 - U\tau$ and $\xi_2 = \gamma_2$, we obtain

$$\Delta p(\tau,\gamma) = \int_{-\infty}^{\infty} \int_{-\infty}^{\infty} (\pi \rho_0 c U) \hat{w}_3(k_1,k_2) g(\gamma_1,k_1,k_2) \times e^{ik_2\gamma_2 - ik_1 U\tau} \, dk_1 \, dk_2 \tag{6}$$

This specifies the loading on the surface as a function of γ_1 and γ_2. When the observer lies in the acoustic farfield of the blade, we may use the approximation that

$$\tau = \left[t - (r_0/c_0) + \eta \cdot \gamma/(r_0 c_0) \right] \Big/ (1 - M_r)$$

When this is used in Eq. (6), it is found that the dependence of $\Delta p(\tau,\gamma)$ on γ_2 is given by $\exp[i(k_2 - \omega' \eta_2/r_0 c_0)\gamma_2]$, where $\omega' = k_1 U/(1 - M_r)$. Consequently, when Eq. (6) is substituted into Eq. (4) and the integral over the span is evaluated between the limits $-\infty < \gamma_2 < \infty$, the result is given by $2\pi\delta(k_2 - \omega' \eta_2/r_0 c_0)$. This is an approximation that is valid, providing the span of the blade b is very much larger than the region of turbulence, $b \gg 2R_2$. Then integrating over k_2 gives in the acoustic far field

$$p_3(\eta,\tau) = \int_{-\infty}^{\infty} \frac{(i\omega'/c_0)(\eta_3/r_0)}{4\pi r_0 |1 - M_r|} \exp\left[-i\omega'(t - r_0/c_0) \right] \times (2\pi)(\pi \rho_0 c U) \hat{w}_3(k_1,k_2) \chi_3 \, dk_1 \tag{7}$$

where

$$\omega' = k_1 U/(1 - M_r), \qquad k_2 = \omega' \eta_2/r_0 c_0$$

and

$$\chi_3(k_1,k_2) = \int_0^c g(\gamma_1,k_1,k_2,) e^{-i(\omega' \eta_1/r_0 c_0)\gamma_1} \, d\gamma_1 \tag{8}$$

The unsteady lift noise (7) must be added to the unsteady thickness noise term that is specified by Glegg et al.[9] as

$$p_\beta(\eta,t) = \frac{\partial^2}{\partial t \, \partial \eta_\beta} \int_{-\infty}^{\infty} \int_0^c \left[\frac{\rho_0 h w_\beta}{4\pi r |1 - M_r|} \right] d\gamma_1 \, d\gamma_2 \tag{9}$$

where tensor notation with $\beta = 1,2$ is used, and h is the thickness distribution over the airfoil planform. Replacing w_β by the inversion integral of $\hat{w}_\beta(k_1,k_2)$, defined as

$$w_\beta(\xi) = \int_{-\infty}^{\infty} \int_{-\infty}^{\infty} \hat{w}_\beta(k_1,k_2) e^{ik_1\xi_1 + ik_2\xi_2} \, dk_1 \, dk_2 \tag{10}$$

and then integrating Eq. (9) over the span give the unsteady thickness noise component in the same form as Eq. (7). The

sum of the unsteady lift and unsteady thickness noise terms is then given by the sum of the three terms $j = 1,2,3$, defined as

$$p_j(\eta,t) = \int_{-\infty}^{\infty} \frac{(i\omega'/c_0)(\eta_j/r_0)}{4\pi r_0} \exp\left[-i\omega'(t - r_0/c_0)\right] \times (2\pi)(\pi\rho_0 c)\hat{w}_j\chi_j \, d\omega' \tag{11}$$

where the variable of integration has been changed to ω', χ_3 is given by Eq. (8), and

$$\chi_\beta = \frac{-i\omega'}{\pi U}\int_0^c \left(\frac{h}{c}\right) e^{i(k_1 - \omega'\eta_1/r_0c_0)\gamma_1} \, d\gamma_1 \qquad \beta = 1,2 \tag{12}$$

The power spectral density of $p_j(\eta,t)$ for a blade in linear motion is

$$S_{pp}^L(\eta,\omega) = \lim_{T\to\infty} \frac{\pi}{T} E\left[|\tilde{p}_T(\eta,\omega)|^2\right] \tag{13}$$

where

$$\tilde{p}_T(\eta,\omega) = \frac{1}{2\pi}\sum_j \int_{-T}^{T} p_j(\eta,t) e^{-i\omega t} \, dt \tag{14}$$

and T is a finite period in observer time. Substituting Eq. (11) into Eq. (14) and integrating over t in the limit $T\to\infty$ gives the Dirac delta function $2\pi\delta(\omega+\omega')$. Then integrating over ω' gives

$$\tilde{p}_T(\eta,\omega) = \sum_j \frac{-(i\omega/c_0)(\eta_j/r_0)}{4\pi r_0} e^{-i\omega r_0/c_0}(2\pi)(\pi\rho_0 c)\hat{w}_j\chi_j \tag{15}$$

where $\hat{w}_j$ and χ_j are evaluated at $k_1 = -\omega(1-M_r)/U$ and $k_2 = -\omega\eta_2/c_0 r_0$.

Incorporating this in Eq. (13) gives

$$S_{pp}^L(\eta,\omega) = \sum_j \sum_i \left[\frac{\omega\rho_0 c}{4\pi c_0 r_0}\right]^2 2\pi^3 U b_e\left(\frac{\eta_i\eta_j}{r_0^2}\right)\chi_i\chi_j^* \times \Psi_{ij}(k_1,k_2)\left[\frac{R_1}{UT}\right] \tag{16}$$

where b_e is defined as the effective span and Ψ_{ij} the effective wavenumber spectrum given by

$$\Psi_{ij}(k_1,k_2) = \frac{2\pi^2}{R_1 b_e} E\left[\hat{w}_i(k_1,k_2)\hat{w}_j^*(k_1,k_2)\right] \tag{17}$$

The quantities Ψ_{ij} and b_e will be discussed in more detail in Sec. V.

In practice, the power spectrum defined by Eq. (16) can only be measured over a finite period $-T < t < T$. In source time, the length of this time interval is $\Delta\tau = 2T/(1-M_r)$, during which the blade will move through the distance $2R_1 = U\Delta\tau$. Consequently, the factor R_1/UT in Eq. (16) is

$$\frac{R_1}{UT} = (1-M_r)^{-1} \tag{18}$$

The power spectrum given by Eq. (16) applies to a blade in linear motion with velocity U through a region of turbulence with effective width b_e. If the turbulence is of uniform intensity over this region then $b_e = 2R_2$. However, in practice this will not be the case and so the effective span b_e has been introduced to normalize the wavenumber spectrum in Eq. (17).

The analysis can be extended to a rotating blade using either the approach given by Paterson and Amiet,[7] for turbulence with a length scale that is much shorter than the rotor diameter, or the approach given by Glegg[9] when wideband data analysis is used. Both methods show that the observed instantaneous power spectrum is nonstationary as a result of the relative motion of the blade and the observer. However, if either of the aforementioned conditions apply, then the instantaneous power spectrum $S_{pp}^I(\boldsymbol{x},\omega,t_1)$ measured at time t_1 by an observer at $\boldsymbol{x}$ is given by the power spectrum of a blade in linear motion at source time τ_1, located at the appropriate position on the rotor disk plane. Consequently, $S_{pp}^I(\boldsymbol{x},\omega,t_1) = S_{pp}^L(\eta,\omega)$, where η is evaluated at the rotor position for source time τ_1. It should be noted here that Glegg's[9] approximation applies when the averaging time T used in Eq. (13) is much shorter than the rotor time period $T_p = \Omega/2\pi$, whereas Paterson and Amiet's[7] approximation applies when $T \gg T_p$ and the averaging in Eq. (13) is carried out, in principle, at fixed rotor positions over many rotor revolutions. A stable estimate of the power spectrum is achieved by averaging the instantaneous spectrum $S_{pp}^I(\boldsymbol{x},\omega,t_1)$ over observer time as

$$S_{pp}(\boldsymbol{x},\omega) = \frac{1}{T_A}\int_0^{T_A} S_{pp}^I(\boldsymbol{x},\omega,t_1) \, dt_1 \tag{19}$$

However, since the instantaneous power spectrum is periodic, a stable average is achieved if $T_A = T_p$. Also since $S_{pp}^I(\boldsymbol{x},\omega,t_1)$ is most easily defined by source position, the averaging in Eq. (19) will be carried out in source time using $S_{pp}^L(\eta,\omega)$ at the appropriate location

$$S_{pp}(\boldsymbol{x},\omega) = \frac{1}{T_p}\int_0^{T_p} \left[S_{pp}^L(\eta,\omega)\right]_{(\eta,\tau_1)}(1-M_r) \, d\tau_1 \tag{20}$$

or alternatively in terms of the azimuthal location ψ_A

$$S_{pp}(\boldsymbol{x},\omega) = \frac{1}{2\pi}\int_0^{2\pi} \left[S_{pp}^L(\eta,\omega)\right]_{\psi_A}(1-M_r) \, d\psi_A \tag{21}$$

This result has assumed that the effective span of the blade immersed in the turbulence b_e is small compared with the rotor diameter. This is reasonable for BWI noise if the blade only intersects a single vortex. If multiple vortices intersect the blade, then the contribution from each should be included independently at the appropriate location on the disk plane as shown by the loci in Fig. 2. Also notice how the Doppler factor $(1-M_r)$ in Eq. (21) cancels with the Doppler factor given by R_1/UT in Eq. (16).

The parameters required to evaluate the measured acoustic spectrum $S_{pp}(\boldsymbol{x},\omega)$ and the spectrum $S_{pp}^L(\eta,\omega)$ are all specified by the rotor design and operating conditions, with the exception of the effective span b_e and the effective turbulence spectrum $\Psi_{ij}(k_1,k_2)$. If the turbulence is isotropic and uniformly distributed over the span b_e, then Ψ_{ij} may be defined in terms of the energy spectrum of the turbulence. In previous work on rotor noise,[6-9] a Von Karman-type energy spectrum has always been assumed. However, before making these assumptions, the turbulence associated with a turbulent tip vortex will be discussed in more detail.

IV. Turbulent Tip Vortex

Turbulent velocity fluctuations associated with tip vortices have been studied with reference to aircraft wake turbulence, and so most of the available information pertains to lifting surfaces in linear motion with well-defined tip loadings. The structure of the tip vortex and how it rolls up is described by Moore and Saffman[11] for a wing with a laminar boundary layer. The vortex core grows with time t and its radius a_0 is approximated by Govindaraju and Saffman[12] as

$$a_0 = k(\tfrac{1}{2}C_L c U t)^{1/2} \tag{22}$$

where C_L is the lift coefficient of each part of a wing of chord c, and U the freestream velocity. The constant k is estimated experimentally to be between 0.1 and 0.3.

The structure of the turbulent vortex is described by Phillips.[13] This differs from the laminar vortex discussed by Moore and Saffman[11] inasmuch that the turbulent boundary

layer shed by the wing is rolled up into the core of the vortex and causes turbulent rather than viscous diffusion to occur. Viscous effects are important in an inner region, but turbulent mixing dominates in the outer region of the core. It has been postulated that it is the turbulent mixing in this region that causes blade wake interaction noise, and to develop a noise prediction scheme based on this premise, it is necessary to evaluate the wavenumber spectrum of this turbulence. The only measurements of the turbulence in a vortex core that have been found in the literature are those by Phillips and Graham.[14] Measurements of this type are difficult since a trailing tip vortex will move in the presence of a velocity-measuring probe. A more stable vortex can be generated using a split-wing arrangement,[14] and this enables more consistent velocity measurements to be obtained. The split-wing arrangement causes a discontinuity in the circulation in an infinite vortex sheet, which rolls up as a double spiral.[15]. This is in contrast to a trailing tip vortex that is caused by the rolling up of a semi-infinite vortex sheet. Therefore, the turbulence intensities measured by Phillips and Graham[14] are expected to be larger than would be found in a trailing tip vortex.

These measurements showed that the maximum turbulence intensities occurred on the centerline of the vortex core and were ~ 2 to 3%. Also the rms velocities were found to be approximately equal in each orthogonal direction, suggesting that the turbulence was approximately isotropic. The turbulence intensities closest to the airfoil were usually larger than those further downstream that correspond to a self-preserving turbulence model, in which the intensity is inversely proportional to the square root of the distance from the vortex generator. The radius of the turbulent vortex core was found to be about 2 to 3 chords, which is 15% larger than prediction by Eq. (22).

For noise-prediction purposes, it is necessary to specify the distribution of the turbulence intensity within the vortex. To a first approximation, this can be evaluated using

$$u = \begin{cases} u_0(1 - r/R_V)(Ut/x_0)^{-1/2} & r < R_V \\ 0 & r > R_V \end{cases} \tag{23}$$

where u_0 is the rms turbulence velocity on the centerline of the vortex at $Ut = x_0$, r is the distance from the center of the vortex, R_V is the effective radius of the vortex, and x_0 is a constant $\approx 45c$ where c is the blade chord. These parameters are unknown for the trailing vortex from a helicopter rotor blade, but u_0 is expected to be smaller than those just described, and it will be assumed to be in the range of $\sim 0.01U$ to $0.02U$. Also, we will approximate R_V by a_0.

The wavenumber spectrum of the turbulence is also required for noise prediction, but unfortunately this was not measured. However, studies of wake turbulence[16,17] show that this can often be modeled using a Von Karman-type energy spectrum with the appropriate turbulence intensity and length scale. The turbulence intensity may be specified using Eq. (23), but no measurements of the length scale are available. It is argued by Phillips[13] that the turbulence in the vortex core is generated in the blade wake, which suggests that the order of magnitude of the turbulence length scale in the vortex core can be estimated from two-dimensional wake measurements. For example, measurements by Wygnanski et al.[17] on a two-dimensional wake from an airfoil at zero angle of attack give the length scale as

$$\frac{L}{\Theta} = 2.1\Delta_0\left(\frac{x - x_0}{\Theta}\right)^{1/2} \tag{24}$$

where x is the distance downstream from the trailing edge, x_0 is the virtual origin of the flow ($x_0 = -380\Theta$ in this case), Θ is the blade boundary-layer momentum thickness, and Δ_0 is found experimentally as 0.32 for this type of wake. The stretching of the turbulence as it is rolled up into the vortex will cause the turbulent eddies to form elliptical shapes that are wrapped around the vortex core. Consequently, the length scale measured azimuthally in the vortex core will exceed the free wake scale given by Eq. (24), whereas the length scale measured radially will be compressed and be less than Eq. (24). Since there are no measurements of the length scale in the vortex core, it will be estimated using Eq. (24) with an empirical correction factor $\gamma \sim 0(1)$ that allows for the stretching of the eddies. Estimates of the turbulence length scale using this approach show that it is very much less than the core size of the vortex given by Eq. (22).

In conclusion, an exact model of the turbulence associated with a trailing vortex has not been found in the literature. However, the order of magnitude of the turbulence intensities, vortex core size, and length scale have been estimated from measurements on a vortex from a split wing, and these will be used to help develop a noise-prediction method using a Von Karman-type energy spectrum.

V. Noise Predictions

To estimate the spectra of BWI noise, a prediction scheme has been developed based on the methods given in Sec. III. The noise is assumed to be produced by the interaction of the blade with the turbulence in the core of trailing vortices of the preceding blades. The locus of the blade vortex intersections, which are shown in Fig. 2, is calculated at equal increments of the wake age angle ψ_W. This specifies the radius and azimuthal angle at which the wake interaction occurs at unequally spaced intervals of ψ_A. The instantaneous noise power spectrum at each location is specified using Eq. (16) and then averaged as a function of azimuth angle by approximating Eq. (21) as

$$S_{pp}(\boldsymbol{x},\omega) = \frac{1}{2\pi}\sum S^L_{pp}(\eta,\omega)\Delta\psi_A(1 - M_r) \tag{25}$$

where $S^L_{pp}(\eta,\omega)$ is the instantaneous spectrum at the azimuth angle ψ_A, and $\Delta\psi_A$ is the increment in azimuth angle between each location in the disk plane. This properly accounts for the change in directionality of the noise caused by the relative position of the blade and the observer and allows for smooth changes in the BVI location. This method cannot be used to calculate impulsive BVI noise levels. These only occur when the trace velocity of the vortex over the blade is supersonic, and so these interactions were eliminated from the calculations. Consequently, only vortices that can be associated with turbulent vortex interaction noise are included.

The effective blade span b_e required in Eq. (16) is evaluated using the model illustrated in Fig. 6. The blade passes through the vortex core at a distance z below the axis. The rms turbulence velocity at a distance x from the mid-point of this intersection is given by Eq. (23), with $r = (x^2 + z^2)^{1/2}$. If we assume that $R_V \gg L$, the effective span of the blade immersed in the vortex core is

$$\begin{aligned} b_e &= \int_{-R_2}^{R_2}\left(1 - \frac{r}{R_V}\right)^2 \mathrm{d}x \\ &= 2R_V\left[h^2 S + \frac{1}{3}S^3 - h^2\,\ell n\left(\frac{1+S}{|h|}\right)\right] \end{aligned} \tag{26}$$

where $R_2 = (R_V^2 - z^2)^{1/2}$, $S^2 = 1 - h^2$, and $h = z/R_V$.

The size of the vortex core is defined using Eq. (22) with C_L approximated by $\alpha 2\pi R_t C_T/Bc$, where α is an empirical constant of order $2 \sim 3$, B is the number of blades, R_t is the blade tip radius, and $Ut = R_t\psi_w$, where ψ_w is the wake age; hence,

$$R_V = \beta R_t(\pi\psi_w C_T/B)^{1/2} \tag{27}$$

where $\beta = k\alpha$. Equation (27) should be used with caution as C_T approaches zero, since for a twisted blade a tip vortex with a core of finite size may still be generated. The purpose of

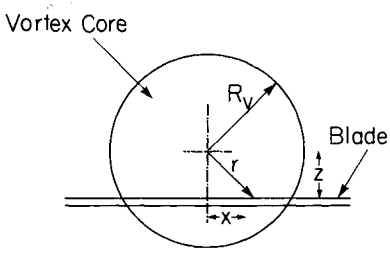

Fig. 6 Interaction of the blade with the vortex core. The blade passes through the core at a distance z below the axis. The rms turbulence velocity is given by $u_c(1-r/R_V)$, where $r=\sqrt{x^2+z^2}$.

Eq. (27) is to identify the scaling of the vortex core radius with thrust, in the absence of more detailed information on the rotor aerodynamics. Also note that $\beta = k\alpha$ is the combination of two empirical constants, where k is used to estimate the vortex core size from Eq. (22) and is ~ 0.1 to 0.3, and α is used to relate the thrust coefficient to the sectional lift coefficient and is ~ 2 to 3. Consequently, the constant β is expected to be 0(1).

The wavenumber spectrum of the turbulence required in Eq. (16) is given by a Von Karman spectrum with the turbulence length scale estimated using Eq. (24). The downstream location of the vortex intersection is given by $x = R_t\psi_w$; hence,

$$L = 0.672\gamma\Theta\left(\frac{R_t\psi_w}{\Theta} + 380\right)^{1/2} \tag{28}$$

where Θ is the momentum thickness of the boundary layer given by $\Theta = 0.037cRe^{-1/5}$ (Re is the Reynolds number based on the chord).

Finally, the turbulence intensity on the centerline of the vortex is given by

$$\frac{u_c}{U} = \frac{u_0}{U}\left(\frac{R_t\psi_A}{x_0}\right)^{-1/2}$$

The experimental measurements described in Sec. IV show that we can expect u_0/U to be ~ 0.01 and the two constants β and γ to be $\sim 0(1)$. In Sec. VI we will discuss the sensitivity of the spectral predictions to each of these parameters.

Finally, it should be noted that Eq. (25) gives the two-sided power spectral density per unit rad/s for a single blade, whereas the results presented by Brooks et al.[1] give the spectrum level for a B bladed rotor. The levels computed using Eq. (25) are therefore corrected by a factor of $4B\pi f_b$, where f_b is the frequency resolution used in data analysis.

VI. Sensitivity of the Results to the Turbulence Parameters

The noise-prediction method described in the preceding section is based on known rotor parameters and four inflow turbulence parameters. The inflow turbulence parameters are

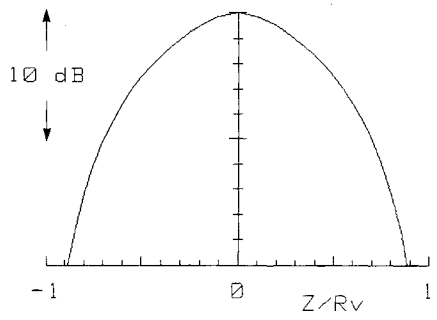

Fig. 7 Sensitivity of BWI noise generation to variations in z/R_V.

the location of the blade vortex intersection (z,R,ψ_A), two nondimensional constants of 0(1) that define the vortex core radius and the turbulence length scale, and the turbulence intensity at the center of the vortex core.

The radial locations of the blade vortex intersections are claimed[5] to be accurately located using the method described in Sec. II, but the axial locations z are known to be imprecise. The ratio z/R_V specifies the effective immersion of the blade in the vortex core, as defined by Eq. (26), and the importance of this parameter to BWI noise generation is illustrated in Fig. 7, which shows $10\log_{10}(3b_e/2R_V)$ as a function of z/R_V. It is clearly seen that small errors in the value of z can cause large dB errors, especially when $|z/R_V| > 0.4$. It would therefore be fortuitous if the spectra computed using this method gave the correct levels for all values of μ and α'_{tip}. However, by rewriting Eq. (1) in the form

$$z = R_t\mu\psi_w(\alpha'_{tip} - \alpha_0)$$

where α_0 is a constant that depends on the rotor operational parameters and using Eq. (27), we find

$$\frac{z}{R_V} = \frac{\mu}{\beta}(\alpha'_{tip} - \alpha_0)\left(\frac{B\psi_w}{\pi C_T}\right)^{1/2} \simeq \frac{20}{\beta}\mu(\alpha'_{tip} - \alpha_0) \tag{29}$$

for $C_T = 0.0044$ and $B = 4$. This scaling is proportional to both the advance ratio μ and the tip-path plane angle α'_{tip} and is in line with the trends shown in Fig. 1. Choosing $\beta = 0.6$ and increasing $|\alpha'_{tip} - \alpha_0|$ from 0 to 6 deg with $\mu = 0.173$ gives a 9 dB reduction in the predicted level, which is of the same order as that in Fig. 1. In the noise-prediction code, a value of $\beta = 0.8$ was found to give a better fit to the experimental data, but this may be a result of errors in estimating the axial displacement of the vortex, which will cause incorrect estimates of α_0 in Eq. (29). Choosing $\beta = 0.8$ may only be applicable to the data set used and the calculation procedure for the vortex locations. However, the arguments just given suggest that although the values of the axial location of the blade vortex intersections cannot be predicted accurately, the scaling with α'_{tip} and μ corresponds with the observed trends in the experimental data.

The turbulence length scale is estimated using Eq. (28) with the unspecified constant $\gamma \sim 0(1)$. This parameter affects the spectral shape and can be adjusted to give the best fit to the experimental data. It was found that values of $\gamma \geq 1.5$ overpredicted the low-frequency part of the spectrum and that values of $\gamma \leq 0.5$ gave spectra that had the wrong slope at high frequencies and underestimated the low frequencies. The best fit was found using $\gamma = 0.8$. In Sec. IV it was assumed that the turbulence was self-preserving and so the turbulence intensity decayed with the square root of the wake age. However, it may also be argued that following the first cutting of the vortex core by a blade, the turbulence is dispersed and subsequent interactions will not be as intense as predicted by this model. This does not have much effect on the predictions of the higher advance ratios (e.g., $\mu = 0.173$) since there are only two significant vortex interactions in the forward sector at this speed. However, at lower advance ratios ($\mu = 0.086$), up to 12 interactions occur and the effect of vortex dispersion tends to reduce the low-frequency content of the spectra. The main effect of introducing vortex dispersion to the model is to reduce the sensitivity of the spectra to variations with tip-path plane angle α'_{tip}. As shown by Eq. (29), vortices with larger wake ages ψ_w will move more with changes in α'_{tip}; hence, if these are eliminated from the model, larger changes in α'_{tip} are required to give the same reductions in level. However, these differences were only found to be of the order of 1 to 2 dB and so the self-preserving model was used.

Finally, the overall level of the spectra will depend on the turbulence intensity. Measurements suggest that this should be in the order of 1 to 2% of the blade tip speed. Comparisons

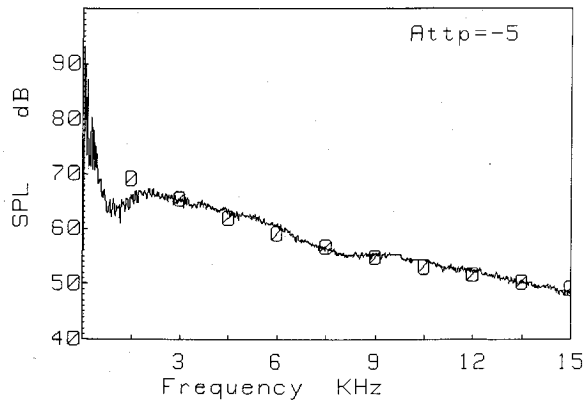

Fig. 8 Comparisons of predictions and measurements of BWI noise.

with experimental data show that the best fit is obtained with a turbulence intensity model given by

$$\frac{u_c}{\Omega R_t} = 0.011\left(\frac{\psi_w R_t}{x_0}\right)^{-1/2} \qquad x_0 = 45c$$

which corresponds to a measured value of 1.1% at 45 chords from the blade tip.

VII. Discussion of Results

An example of the comparison of the predicted results with the measurements presented by Brooks et al.[18] is shown in Fig. 8 for the advance ratio and tip-path plane angle illustrated in Fig. 1. There is a reasonable fit between the measurements and the predictions between 2 and 8 kHz, where BWI dominates. Over the complete data set,[18] errors of up to 4 dB between the predictions and measurements were found in the 3 to 4.5 kHz range for advance ratios of $\mu = 0.086$ and 0.173. However, for the highest advance ratio, $\mu = 0.283$, the scaling of the data with variations in α'_{ttp} and μ was not completely consistent with the aerodynamic model described in Sec. II. The predicted noise levels were of the correct magnitude when α'_{ttp} was small, but were in error by up to 10 dB at large tip-path plane angles.

The major inconsistency of this prediction method is well illustrated by Fig. 8. This shows that the measured spectrum of BWI noise has a distinct peak at 2.5 kHz, which is not predicted. This peak is often hidden in spectra that include significant levels of BVI, but is clearly identifiable at the larger tip-path plane angles. The shape of this spectrum cannot be modeled using a Von Karman energy spectrum for the turbulence in the vortex core. Better results could be obtained at low frequencies by significantly reducing the turbulence length scale, but if this is done, the high-frequency part of the spectrum is almost flat and grossly overpredicts the measurements. This suggests that a turbulence model with less energy at high frequencies may be expected to give a more accurate fit to the spectral shape. These types of energy spectrum are found in boundary-layer flows, but are inconsistent with the measurements of wake turbulence described by Wygnanski et al.[17] It has been assumed here that the turbulence spectrum is the same over the complete vortex core. However, this may not be the case and large-scale structures may be the dominant feature of the flow when the blade passes through the edge of the vortex and may be responsible for the observed trends.

The purpose of this paper has been to show that a model for BWI noise based on the concept of blade vortex interactions in the forward sector of the rotor can reproduce the experimental observations. The turbulence associated with the vortex has been estimated from wind-tunnel measurements, and only small adjustments to these have been required to give the correct radiated noise levels in the mid-frequency range. This suggests that the model is reasonable, but more detailed experimental observation, including flow visualization, would help to confirm these ideas. The major limitation of the method is the accuracy with which the vortex intersections can be calculated and the model used for the spectrum of the turbulence in the vortex core. More information about these quantities is required before better noise predictions can be obtained.

Acknowledgment

This work was supported by NASA Grant NAG-1-715. The author would like to thank F. Farassat and T. F. Brooks for useful discussions during the course of this work.

References

[1]Brooks, T. F., Marcolini, M. A., and Pope, D. S., "Main Rotor Noise Study in the DNW," AHS Specialist Meeting on Aerodynamics and Aeroacoustics, Arlington, TX, Feb. 25-27, 1987.

[2]Brooks, T. F., and Martin, R. M., "Results of the 1986 NASA/FAA/DFVLR Main Rotor Test Entry in the German-Dutch Wind Tunnel (DNW)," NASA TM-100507, 1987.

[3]Munch, C. L., Patterson, R. W., and Day, H., "Rotor Broadband Noise Resulting from Tip Vortex/Blade Interaction," Sikorsky Aircraft Rept. AD-A020692, 1976, NASA STAC #76N26207.

[4]Marcolini, M. A., and Brooks, T. F., "Rotor Noise Measurement Using a Directional Microphone Array," AIAA Paper 87-2746, 1987.

[5]Egolf, T. A., and Landgrebe, A. J., "Helicopter Rotor Wake Geometry and Its Influence in Forward Flight," Vols. 1 and 2, NASA CR 3726 and 3727, Oct. 1983.

[6]Amiet, R. K., "Acoustic Radiation From an Airfoil in a Turbulent Stream," *Journal of Sound and Vibration*, Vol. 41, 1975, pp. 407-420.

[7]Paterson, R. W., and Amiet, R. K., "Noise of a Model Helicopter Rotor Due to Ingestion of Turbulence," NASA CR-3213, 1979.

[8]Glegg, S. A. L., "The Significance of Unsteady Thickness Noise Sources," *AIAA Journal*, Vol. 25, No. 6, 1987, pp. 839-844.

[9]Glegg, S. A. L., Baxter, S. M., and Glendinning, A. G., "The Prediction of Broadband Rotor Noise from Wind Turbines," *Journal of Sound and Vibration*, Vol. 118, No. 2, 1987, pp. 217-239.

[10]Homicz, G. F., and George, A. R., "Broadband and Discrete Frequency Radiation from Subsonic Rotors," *Journal of Sound and Vibration*, Vol. 36, 1974, pp. 151-177.

[11]Moore, D. W., and Saffman, P. G., "Axial Flow in Laminar Trailing Vortices," *Proceedings of the Royal Society, (London)*, Vol. A333, 1973, pp. 491-508.

[12]Govindaraju, S. P., and Saffman, P. G., "Flow in a Turbulent Trailing Vortex," *Physics of Fluids*, Vol. 14, No. 10, 1971, p. 2074.

[13]Phillips, W. R. C., "The Turbulent Trailing Vortex During Roll-up," *Journal of Fluid Mechanics*, Vol. 105, 1981, p. 451.

[14]Phillips, W. R. C., and Graham, J. A. H., "Reynolds-Stress Measurements in a Turbulent Trailing Vortex," *Journal of Fluid Mechanics*, Vol. 147, 1984, p. 353

[15]Pullin, D. I., and Phillips, W. R. C., "On a Generalization of Kadens Problem," *Journal of Fluid Mechanics*, Vol. 104, 1981, p. 45.

[16]Champagne, F. H., "The Fine Scale Structure of the Turbulent Velocity Field," *Journal of Fluid Mechanics*, Vol. 86, 1978, p. 67.

[17]Wygnanski, I., Champagne, F., and Marasli, B., "On the Large-Scale Structures in Two-Dimensional, Small Deficit, Turbulent Wakes," *Journal of Fluid Mechanics*, Vol. 168, 1986, p. 31.

[18]Brooks, T. F., Jolly, J. R., Jr., and Marcollini, M. A., "Helicopter Main Rotor Noise," NASA TP 2825, Aug. 1988.